ELSEVIER

Earth and Planetary Science Letters 199 (2002) 111–126

EPSL

www.elsevier.com/locate/epsl

Archean sulfide inclusions in Paleozoic zircon megacrysts from the Mir kimberlite, Yakutia: implications for the dating of diamonds

Z.V. Spetsius [a], E.A. Belousova [b], W.L. Griffin [b,c], Suzanne Y. O'Reilly [b,*], N.J. Pearson [b]

[a] *Institute of Diamond Industry, ALROSA Co. Ltd., Mirny, Yakutia 678170, Russia*
[b] *GEMOC ARC National Key Centre, Department of Earth and Planetary Sciences, Macquarie University, Sydney, NSW 2109, Australia*
[c] *CSIRO Exploration and Mining, P.O. Box 126, North Ryde, NSW 1670, Australia*

Received 5 September 2001; accepted 15 February 2002

Abstract

Zircon megacrysts from the Mir kimberlite, Yakutia, contain inclusions of chromite, chrome diopside, magnesian olivine, Ni-rich monosulfide solid solution and phlogopite. The mineral chemistry of the inclusion suite suggests that the zircons grew in a metasomatized peridotite matrix. Twenty-three zircons were chosen for U–Pb dating, Hf isotope and trace element determinations. The trace element data are typical of kimberlitic zircons worldwide. LAM-ICPMS U–Pb dating yields a weighted mean $^{206}Pb/^{236}U$ age of 353.6 ± 2.5 Ma. Hf isotope measurements by LAM-MC-ICPMS yield ε_{Hf} values of 3.0–9.2, and model ages (T_{DM}) of 600–800 Ma. These data constrain the crystallization of the zircons to between 350 and 600 Ma. However, LAM-MC-ICPMS microanalysis of Os isotopes in sulfides included in three zircons yields T_{RD} model ages of 2.37–2.92 Ga (T_{MA} = 2.39–3.19 Ga). To explain the discordance between the ages of the zircons and their sulfide inclusions, we suggest that these zircons grew in a metasomatized peridotite, which contained sulfides that were residual from ancient melting events. These sulfides, together with other peridotite phases, were trapped in the metasomatic zircon with little modification of their elemental or isotopic composition. This model has important implications for the interpretation of Re–Os model ages of sulfide inclusions in diamonds. Diamonds also could capture and preserve older sulfides during their growth or regrowth in mantle rocks, and the inclusions therefore do not necessarily date the formation of the diamond.

Keywords: kimberlite; zircon; Mir Pipe; U–Pb; hafnium; isotope ratios; Re/Os; diamond

1. Introduction

The Mir kimberlite of Yakutia was the first diamondiferous pipe discovered on the Siberian platform; it is one of the richest in the world, and has been mined since 1956. Mantle xenoliths

* Corresponding author. Tel.: +61-2-9850-8953; Fax: +61-2-9850-8362.
E-mail address: sue.oreilly@mq.edu.au (S.Y. O'Reilly).

0012-821X/02/$ – see front matter
PII: S0012-821X(02)00539-3

and megacryst minerals (including zircons) from this pipe were first described by Bobrievich et al. [1]. The mineralogy and paragenetic associations of inclusions in the zircons were investigated later in detail [2,3]. Zircons from the Mir kimberlites have been dated by conventional U–Pb methods [4] to 361.5 Ma.

Mineral inclusions in the zircons from Mir represent an ultramafic association of chromites and rare Mg-rich olivine, phlogopite and chrome diopside. In contrast, the analogous zircon megacrysts that are widespread in the kimberlites of South Africa [5–7] commonly are intergrown with other phases of the low-Cr megacryst site (ilmenite, phlogopite, Fe-rich olivine). To understand the significance of these differences, we need to know more about the age and isotopic composition of the zircons and their inclusions. This information also may help us to understand the evolution of the subcontinental lithospheric mantle and diamond formation.

The discovery of sulfide inclusions in some grains of zircon from Mir was the motivation for this new investigation of the zircon population, using new techniques for U–Pb and Hf isotope analysis, and with special attention to Re–Os dating of the rare sulfide inclusions.

2. Sample description

The zircons were recovered from the host kimberlite during the diamond separation process. Zircons in the Mir kimberlite are up to 2 cm in diameter, and show a range of shapes; the grains analyzed here are 4–12 mm across. Color ranges from white and pale pink (nearly colorless) to shades of amber and brown. Many grains have frosted or white baddeleyite-coated surfaces. Twenty-three zircon megacrysts, mostly with inclusions, were chosen from a large collection. These grains are characterized by an almost complete absence of crystal faces; they are typically rounded to subrounded, and display a large range of colors with a predominance of yellow and brown.

The zircon grains were mounted in epoxy discs and polished. The sections were mapped using cathodoluminescence (CL) imaging, and then used for electron microprobe analysis, trace element analysis, U–Pb dating, and Hf isotope determinations. Most grains were subsequently repolished to expose the sulfide inclusions for elemental analysis and Re–Os dating.

3. Analytical methods

3.1. Major element analysis

Major element compositions of silicate and oxide inclusions in the zircons were determined with a Superprobe JXA-8800R electron microprobe at the ALROSA Co Ltd., Mirny, Yakutia, Russia. Compositions of sulfide inclusions were analyzed on a CAMEBAX SX50 electron microprobe at the GEMOC ARC National Key Centre, Macquarie University, Sydney, Australia. In both cases natural minerals and synthetic were used as standards. Analytical conditions included an accelerating voltage of 15 keV, a beam current of 20 nA, beam size of 5 μm, and counting time of 20 s for all elements. All analyses underwent a full ZAF correction.

3.2. Trace element analysis

Trace elements have been analyzed using a 266 nm UV laser ablation microprobe (LAM) coupled to an Agilent HP4500 inductively coupled mass spectrometer at GEMOC. Detailed descriptions of instrumentation, analytical and calibration procedures are given by Norman et al. [8,10]. All analyses have been carried out with a pulse rate of 10 Hz and a beam energy of about 1 mJ per pulse, producing a spatial resolution of ca. 80 μm. Quantitative results for 26 elements were obtained through calibration of relative element sensitivities using the NIST-610 glass as external standard with the recommended values of Norman et al. [8], and normalization of each analysis to the electron-probe data for Hf as an internal standard; an average value of 1.28 wt% HfO_2 in zircon from the Mir kimberlite was taken from Belousova [9]. Detection limits are typically less than 0.02 ppm for the rare earth elements (REEs), Y,

Nb, Ta, Th and U. The precision and accuracy of these analyses are 0.5–2% for REE, Y, Sr, Nb, Ta, Th and U at the ppm concentration level, and from 3 to 6% for Mn, P, Fe, Ti and Sn.

3.3. U–Pb dating

Grain mounts containing the samples and GEMOC GJ1 zircon standard were cleaned in 2 N nitric acid for ca. 1 h prior to analysis. LAM-ICPMS analyses were performed using a custom-built 266 nm UV LAM [8] coupled to an Agilent HP4500, series 300, ICPMS at GEMOC. ICPMS operating conditions and data acquisition parameters are given by Belousova et al. [11].

Samples and standard were ablated in He to minimize deposition of ablation products around ablation sites and improve sample transport efficiency; it also gives more stable signals and more reproducible Pb/U fractionation. To minimize dynamic U/Pb fractionation as the laser beam penetrates into the sample [12], analyses were performed with the laser focused above the sample (typically ~200 μm). Identical laser operating conditions were rigorously maintained throughout each run of 20 analyzes to ensure constant U/Pb fractionation. Ablation pit diameter was generally about 80 μm.

Samples were analyzed in separate 'runs' of 20 analyses comprising 12 analyses of unknowns bracketed by four analyses of the GEMOC GJ1 zircon standard, a gem quality zircon that contains ca. 260 ppm U; multiple thermal ion mass spectroscopy (TIMS) analyses show it to be 608.5 ± 0.4 Ma old ($^{207}Pb/^{206}Pb$ age) and very slightly discordant (F. Corfu, personal communication).

Each analysis was ~180 s, with gas background measurements being taken over the first ~60 s, prior to initiation of ablation. Data were acquired on five masses (206–208, 232, 235) with short dwell times to provide quasi-simultaneous measurement of the five masses and optimum precision. Time-resolved signals (i.e. signals as a function of time, which is a proxy for ablation depth) allow isotopic heterogeneity within the ablation volume to be clearly identified (e.g. zones of Pb loss or common Pb related to fractures or areas of radiation damage; also inclusions, inherited cores, etc.).

Raw data were processed using GLITTER, an in-house on-line data reduction program. $^{207}Pb/^{206}Pb$, $^{208}Pb/^{232}Th$, $^{206}Pb/^{238}U$ and $^{207}Pb/^{235}U$ ($^{235}U = {}^{238}U/137.88$) ratios were calculated for each mass sweep and the time-resolved ratios for each analysis were then carefully examined. Optimal signal intervals for the background and ablation data were selected for each sample and automatically matched with identical time intervals for the standard zircon analyses, thus correcting for the effects of ablation/transport-related U/Pb fractionation and mass bias of the mass spectrometer. Net background-corrected count rates for each isotope were used for calculation of sample ages. Concordia ages were determined using Isoplot 2.32 [13].

The ^{204}Pb isotope cannot be precisely measured with this technique, due to a combination of low

Table 1
Precision and accuracy of LAM-ICPMS data compared with TIMS data on some well-characterized zircons

	TIMS 207/206	206/238	MSWD	207/235	MSWD	207/206	MSWD
UQ-Z5	1143 ± 1	Machado and Gauthier [43]; $n = 9$					
$n = 14$		1138 ± 17	5.5	1137 ± 11	5.7	1134 ± 11	0.32
$n = 33$		1136 ± 14	4.7	1134 ± 11	5	**1135 ± 9**	6.2
Temora	417	L. Black (personal communication, 2000)					
$n = 11$		**416.7 ± 2.9**[a]	0.69	414.7 ± 3.7	0.35	406 ± 23	0.31
91500	1065.4	Wiedenbeck et al. [44]; $n = 11$					
$n = 75$		1051 ± 7	4.4	1056 ± 3.3	3.1	**1066 ± 5**	0.72
Mud Tank	734 ± 32	Black and Gulson [45]; $n = 5$					
$n = 67$		**736 ± 3**	2.9	737 ± 3	2.6	740 ± 7	0.46

[a] LAM-ICPMS 206/238 ages preferred for samples with age < 1 Ga.
207/206 ages preferred for older samples.

signal and interference from small amounts of ^{204}Hg in the Ar gas supply. Therefore no correction for common Pb has been made; as will shown below, several grains can be shown to contain common Pb, and have been rejected.

This methodology gives $^{206}Pb/^{238}U$ and $^{207}Pb/^{206}Pb$ ages with precision and accuracy comparable to that of most ion-probe data; the precision of $^{207}Pb/^{235}U$ ages is somewhat lower. The precision and accuracy obtained with this technique are illustrated by comparison with TIMS data for some well-characterized zircons (Table 1, [11]).

3.4. Hf isotope determination

Hf isotope analyses were carried out in situ with a Merchantek EO LUV 266nm laser-ablation microprobe, attached to an Nu plasma multi-collector (MC) ICPMS at GEMOC. The methodology is described in detail by Griffin et al. [14]. Interference of ^{176}Lu on ^{176}Hf has been corrected by measuring the intensity of the interference-free ^{175}Lu isotope and using the recommended $^{176}Lu/^{175}Lu = 0.02669$ [15] to calculate $^{176}Lu/^{177}Hf$. Similarly, the interference of ^{176}Yb on ^{176}Hf has been corrected by measuring the interference-free ^{172}Yb isotope and using $^{176}Yb/^{172}Yb$ to calculate $^{176}Yb/^{177}Hf$. The appropriate value of $^{176}Yb/^{172}Yb$ was determined by spiking the JMC475 Hf standard with Yb, and determining the value of $^{176}Yb/^{172}Yb$ (0.58669) required to yield the value of $^{176}Hf/^{177}Hf$ obtained on the pure Hf solution. Table 2 shows data for analyses of the Yb-spiked JMC475 solutions with $^{176}Yb/^{176}Hf$ up to 0.96 ($^{176}Yb/^{177}Hf \approx 0.26$). These data illustrate the precision and accuracy obtainable on the $^{176}Hf/^{177}Hf$ ratio, despite the severe corrections on ^{176}Hf. Most LAM analyses were carried out in Ar carrier gas with a beam diameter of ca. 80 μm, a 10 Hz repetition time, and energies of 0.6–1.3 mJ/pulse. Typical ablation times were 80–120 s, resulting in pits 40–60 μm deep. The precision and accuracy of these analyses is illustrated by the analyses of zircon standards in Table 2, and are discussed in detail by Griffin et al. [14].

For the calculation of ε_{Hf} values we have adopted the chondritic values of Blichert-Toft and Albarede [16]. The calculated model ages are based on the depleted-mantle source model described by Griffin et al. [14].

3.5. Re–Os determination

Re–Os isotopes were analyzed using a Merchantek LUV266 laser microprobe with a modified ablation cell, attached to the Nu plasma MC-ICPMS at GEMOC. All ablations were carried out using He as the carrier gas. Most analyses were done at 4 Hz repetition rate and energies of ca. 2 mJ/pulse; typical pit diameters were 50–

Table 2
Analyses of Lu–Hf standard solutions and standard zircons

Sample	No. analyses	Yb (ppm)	Lu (ppm)	Hf (ppm)	$^{176}Lu/^{177}Hf$	$^{176}Yb/^{177}Hf$	$^{176}Hf/^{177}Hf$	±2 S.D.	Hf (V)
JMC475 Hf	169			0.1–1.0			0.28216	0.000026	5–18[b]
JMC475 Hf (+Yb)	17	0.08		1		0.055	0.282167	0.00002	9–18
JMC475 Hf (+Yb)	9	0.04		0.105		0.26	0.282154	0.000053	0.8–4.0
Zircon 91500	60	62.5	13.9 12.4[a]		0.0003		0.282297	0.000044	1–6
TIMS	7		12	5895	0.00029		0.28229	0.000014	
Zircon 61308									
high Lu, Yb	13				0.00162	0.05105	0.282991	0.000094	2–6
low Lu, Yb	9				0.00021	0.00615	0.282968	0.000111	2–6
all	22	352	78		0.00104	0.03269	0.282982	0.000102	2–6
TIMS	9		83	5658	0.00207	n.a.	0.282975	0.00005	

Yb and Lu concentrations of zircons by LAM-ICPMS.
TIMS data from Wiedenbeck et al. [44].
[a] Lu calculated from $^{176}Lu/^{177}Hf$ and given Hf content.
[b] 5–10 V for 0.1 ppm solution using MCN6000; 9–18 V for 1 ppm solution using Meinhard nebulizer.

Table 3
Analyses of Re–Os standard solutions and PGE-A sulfide standard

Standard		Collector 1	$^{192}Os/^{188}Os$	1 S.E.	$^{190}Os/^{188}Os$	1 S.E.	$^{189}Os/^{188}Os$	1 S.E.	$^{187}Os/^{188}Os$	1 S.E.	$^{186}Os/^{188}Os$	1 S.E.
GEMOC JM Os	avge $n=12$	F	3.07989	6.69E-05	1.98273	3.85E-05	1.21942	2.65E-05	0.18363	2.19E-05	0.12087	1.71E-05
	2 S.D.		5.41E-04		4.05E-04		2.14E-04		1.31E-04		1.73E-03	
PGE-A	avge $n=67$	F+IC	3.08033	1.23E-03	1.98072	6.06E-04	1.21950	5.02E-04	0.10638	6.87E-05	nd	nd
	2 S.D.		1.35E-02		7.49E-03		4.07E-03		4.76E-04		nd	

80 μm. The analytical procedures have been described in detail by Pearson et al. ([17]; also see www.es.mq.edu/GEMOC/). A dry aerosol of Ir, produced by a CETAC MCN6000 desolvating nebulizer, was bled into the gas line between the ablation cell and the ICPMS to provide a mass-bias correction with a precision independent of the abundance of Os in the sample. The total Ir signal is typically 2–3 V. Pearson et al. [17] have demonstrated that this procedure provides a significant improvement to precision relative to the use of the Os isotopes of the sample itself, especially for samples with low signals. Masses 188–194 were measured in Faraday cups, and masses 185 and 187 were measured in ETP ion counters. The measurement of ^{185}Re is used to correct for the overlap of ^{187}Re on ^{187}Os [17].

The ion counters were calibrated initially against the Faraday cups and one another using a two-cycle analysis of a standard Os solution, rather than the sequential analysis of Ir+Os and Re+Ir solutions used by Pearson et al. [17]. During ablation runs, a standard NiS bead with 200 ppm Os and Pt (platinum group element-A (PGE-A)) was analyzed between samples, to monitor and correct any drift in the ion counters. These corrections typically were less than 1% over a long day's analytical session. The data were collected using the Nu plasma time-resolved software, which allows the selection of the most stable intervals of the signal for integration.

The precision and accuracy of the method are discussed in detail by Pearson et al. [17]. Under ideal circumstances (sulfides >50 μm diameter, $>$ ca. 40 ppm Os), an internal precision for $^{187}Os/^{188}Os$ of 0.1–0.3% is routinely obtained (Table 2); for smaller grains or lower Os contents (to 1–5 ppm), precision of 1–2% is routine. The external reproducibility of $^{187}Os/^{188}Os$ for the PGE-A standard over several months is ± 0.0004 (2 S.D., Table 3). Os and Pt contents have been estimated semiquantitatively by comparison of sample signals with the signals on the PGE-S standard under similar conditions. The $^{187}Re/^{188}Os$ ratio is measured directly; Re concentrations are not determined independently, as the PGE-A standard does not contain Re.

4. Results

Zircons were mounted in epoxy discs and polished. CL imaging was used to examine internal structures and heterogeneities in the zircons [18,19]. The zircons show yellowish, pinkish and bluish CL colors, with bluish hues predominating. Most of the studied grains are homogenous in CL color and five crystals show blocky and broad featureless bands. Only two grains show evidence of complicated growth histories in the form of complex zoning patterns. Inclusions of chromite or sulfide commonly occur in zones with different CL colors than the surrounding zircon.

4.1. Trace element data

The trace element compositions of the zircons are given in Table 4. Adjacent zones with different CL colors (blue and yellow) in three zircons showed no obvious difference in trace element contents. The chondrite-normalized patterns of the Mir zircons lie generally within the band defined by zircons from other kimberlites in Southern Africa, Yakutia and Australia (Fig. 3,

Table 4
LAM-ICPMS analyses of trace elements in zircons from Mir kimberlites in ppm

	P	Ti	Mn	Fe	Sr	Y	Nb	Sn	La	Ce	Pr	Nd	Sm	Eu	Gd	Tb	Dy	Ho	Er	Tm	Yb	Lu	Ta	Th	U
Mir-1	52.9	11.4	0.66	23.0	0.83	20.7	2.84	0.49	0.126	1.05	0.05	0.48	0.35	0.18	0.93	0.24	2.25	0.67	2.45	0.43	3.60	0.67	2.14	1.65	6.12
Mir-2	28.8	7.79	0.19	3.56	0.06	53.7	2.64	0.10	< 0.004	1.03	0.01	0.12	0.30	0.25	1.78	0.56	6.24	1.93	7.41	1.37	12.10	2.16	2.03	2.56	10.6
Mir-3	37.5	9.76	0.22	3.14	0.06	39.2	2.45	0.11	< 0.004	0.96	0.01	3.64	0.38	0.31	1.83	0.50	4.98	1.43	5.15	0.90	7.58	1.34	1.72	2.72	8.14
Mir-4	39.9	8.12	0.22	3.07	0.05	22.2	2.05	0.08	< 0.004	0.68	0.004	0.11	0.17	0.13	0.81	0.24	2.65	0.80	3.11	0.61	5.34	0.98	1.63	1.30	5.84
Mir-6	45.2	7.58	0.20	5.17	0.05	6.12	2.58	0.09	< 0.004	0.61	0.004	0.03	0.05	0.04	0.22	0.06	0.66	0.21	0.75	0.14	1.27	0.25	2.32	0.99	5.20
Mir-7	41.3	7.00	0.13	3.17	0.06	28.2	2.37	0.12	0.005	0.99	0.01	0.13	0.24	0.14	0.96	0.29	3.36	0.99	3.90	0.72	6.35	1.18	1.85	1.92	8.67
Mir-8	60.1	7.05	< 0.12	4.96	0.06	33.0	2.56	0.11	< 0.003	0.88	0.01	0.14	0.27	0.19	1.04	0.36	3.55	1.17	4.65	0.87	7.75	1.42	2.35	1.91	9.05
Mir-9	47.9	7.03	0.13	< 2.38	0.04	28.6	2.50	0.11	< 0.004	0.91	0.01	0.15	0.23	0.18	0.95	0.30	3.28	1.01	4.03	0.78	7.02	1.37	1.89	1.87	8.21
Mir-10	54.6	7.22	0.20	3.15	0.06	31.4	3.02	0.11	0.003	1.16	0.01	0.14	0.21	0.19	1.05	0.32	3.56	1.13	4.32	0.83	7.63	1.46	2.58	2.44	10.4
Mir-11	47.5	5.81	0.28	4.20	0.05	24.8	2.35	0.13	< 0.004	0.93	0.09	0.08	0.24	0.15	0.79	0.27	2.91	0.87	3.31	0.62	5.41	1.02	1.97	1.74	7.73
Mir-12	56.3	7.68	< 0.13	< 2.90	0.06	27.6	2.61	0.10	< 0.003	0.89	0.01	0.12	0.17	0.15	0.98	0.27	3.12	0.99	3.87	0.74	6.64	1.31	2.12	1.74	7.91
Mir-13	39.3	7.74	0.24	2.91	0.07	55.7	2.97	0.09	< 0.004	1.30	0.02	0.25	0.53	0.40	2.44	0.71	7.15	2.05	7.46	1.34	10.87	1.96	2.24	3.58	11.0
Mir-14	34.9	5.71	< 0.09	1.98	0.05	9.22	3.31	0.12	< 0.004	0.92	0.01	0.17	0.14	0.09	0.50	0.12	1.12	0.33	1.18	0.22	1.69	0.29	2.17	2.66	4.61
Mir-15	46.3	8.70	2.30	71.2	0.28	5.13	1.98	0.67	0.038	0.49	0.01	0.09	0.03	0.04	0.21	0.05	0.55	0.15	0.62	0.11	1.10	0.21	2.05	0.65	3.30
Mir-16	49.0	8.52	0.30	5.19	0.04	22.0	2.10	0.09	< 0.005	0.77	0.01	0.11	0.21	0.13	0.77	0.25	2.51	0.78	3.04	0.57	5.02	0.92	1.46	1.41	6.36
Mir-17	29.9	8.29	0.12	2.67	0.04	29.1	1.77	0.09	< 0.003	0.67	0.01	0.08	0.18	0.14	0.84	0.28	3.25	1.04	4.12	0.73	6.24	1.12	1.51	1.32	5.92
Mir-18	41.9	11.4	0.15	4.34	0.24	41.3	2.58	0.11	0.056	1.19	0.02	0.34	0.49	0.37	1.98	0.55	5.17	1.50	5.45	0.99	8.53	1.51	1.74	3.05	8.62
Mir-19A	42.8	6.79	0.16	3.71	0.04	4.79	1.50	0.08	< 0.003	0.43	< 0.003	< 0.01	0.04	0.01	0.17	0.06	0.57	0.18	0.65	0.12	1.03	0.18	1.77	0.69	3.29
Mir-19B	47.4	6.56	0.22	4.99	0.05	4.76	2.10	0.11	< 0.003	0.41	< 0.003	< 0.02	0.04	0.03	0.17	0.05	0.53	0.17	0.64	0.11	0.94	0.19	2.07	0.68	3.39
Mir-20	23.8	8.75	0.30	2.56	0.06	33.9	1.82	0.08	< 0.004	0.79	0.01	0.11	0.23	0.16	1.13	0.36	3.96	1.22	4.63	0.86	7.11	1.30	1.53	1.62	7.45
Mir-21A	35.6	8.08	0.21	2.36	0.05	21.3	2.20	0.09	< 0.003	0.81	0.01	0.10	0.17	0.13	0.74	0.24	2.48	0.77	2.90	0.56	4.76	0.88	1.62	1.48	6.47
Mir-21B	40.2	7.67	0.24	3.65	0.05	22.3	2.22	0.08	< 0.002	0.76	0.01	0.09	0.20	0.13	0.91	0.25	2.66	0.81	3.09	0.58	5.21	0.97	1.67	1.45	6.36
Mir-23	62.7	8.50	0.31	< 2.65	0.06	14.8	3.36	0.10	0.005	0.77	0.01	0.05	0.08	0.07	0.42	0.15	1.59	0.52	2.15	0.41	3.82	0.75	3.43	1.47	6.73
Mir-24A	27.3	8.39	0.20	3.43	0.05	31.7	1.94	0.08	< 0.004	0.83	0.01	0.10	0.22	0.15	0.94	0.31	3.44	1.13	4.57	0.86	7.68	1.45	1.63	1.65	7.48
Mir-24B	44.3	7.25	0.40	5.92	0.05	14.6	2.55	0.08	< 0.004	0.81	0.01	0.06	0.13	0.09	0.47	0.15	1.58	0.51	2.02	0.36	3.35	0.63	2.24	1.41	6.79
Mir-25	40.0	6.85	< 0.11	< 2.36	0.05	6.44	2.99	0.07	< 0.003	0.60	0.003	0.03	0.05	0.04	0.17	0.07	0.66	0.23	0.92	0.17	1.57	0.29	2.81	0.97	5.00
MDL	2.55	0.22	0.11	2.40	0.01	0.01	0.01	0.02	0.003	0.003	0.003	0.02	0.02	0.01	0.02	0.004	0.01	0.003	0.01	0.003	0.02	0.003	0.003	0.003	0.003

MDL = minimum detection limit.

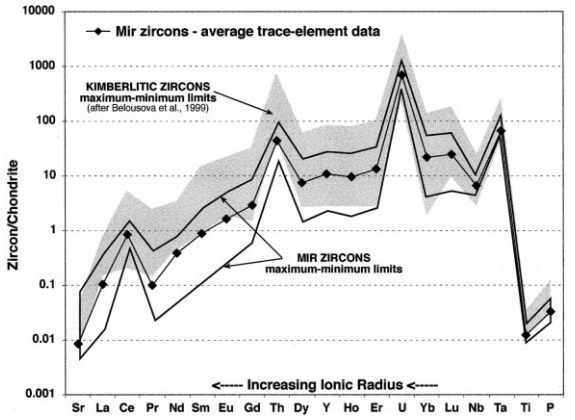

Fig. 1. Trace element (LAM-ICPMS) data for the zircon population from the Mir kimberlite, compared with those for the kimberlitic zircons of other localities.

[18,19]). However, the Mir zircon population has slightly lower concentrations of almost all trace elements (Fig. 1) than zircon populations from other kimberlites worldwide. The lower mean values for the light REE also reflect the higher sensitivity of the instrument used during this study. The Mir zircons have lower contents of Th than most zircons from other kimberlites of Siberia and South Africa [18].

4.2. Mineral inclusions

The zircon grains studied here contain inclusions of chromite, clinopyroxene and sulfide. Inclusions of chromite are most abundant; the number of inclusions in single zircon grains varies from 1 to >10 crystals. The chromites occur as octahedral crystals 30–200 μm across (Fig. 2) and rarely up to 0.5 mm. The compositions of chromite inclusions show little variation either within a single zircon or between zircon grains (Table 5). Analyses of the central and outer parts of chromites from three zircon grains did not show detectable zoning. All analyzed chromites have high Cr_2O_3 contents (45.5–50.0 wt%), a narrow range of MgO (8.0–9.0 wt%) and high contents of TiO_2 (2.8–3.3 wt%). Chromites with similar high Ti compositions are common as macrocrysts in kimberlites [20]. Schulze [21] has shown that they can be derived from the disaggregation of garnet–chromite lherzolites, in which the garnets also show the high Ti contents characteristic of metasomatized harzburgites and lherzolites [22]. However, it should be noted that garnet has not been found as inclusions in zircons from Mir or other pipes in Yakutia.

A clinopyroxene inclusion in zircon #10 is oval and 0.20 mm long. It is a chrome diopside, high in MgO, CaO and Cr_2O_3 (>1.7 wt%, Table 5), and low in Na_2O and TiO_2. The Na_2O content increases slightly from the core to the rim of the inclusion (an. #11 and #13, Table 5). This inclusion is similar in composition to clinopyroxenes from the garnet lherzolite and garnet websterite xenoliths from this pipe [23]. Ponomarenko [2] described an olivine inclusion (Fo = 92.2%) in a zircon megacryst from Mir (Table 5); its composition is typical of olivine in lherzolite xenoliths from this pipe [23].

Sulfide inclusions were found in three zircons. They show well-developed negative zircon crystal

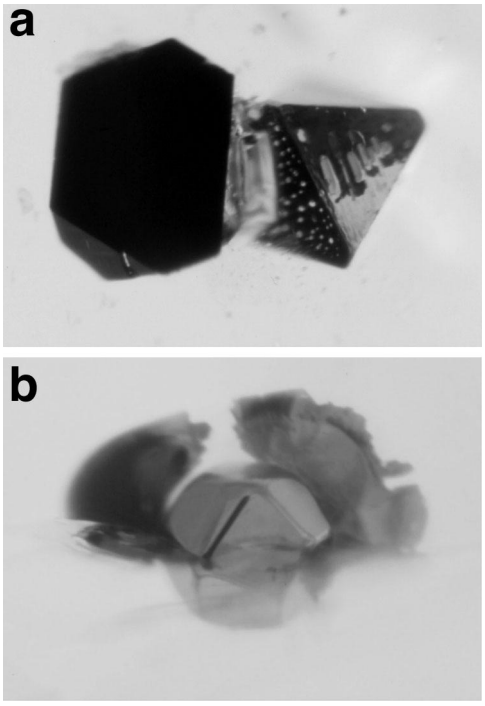

Fig. 2. Inclusions in zircon megacrysts from the Mir kimberlite pipe. (a) Intergrowth of two chromite octahedra (ca. 150 μm across) in sample Zr-21. (b) Euhedral sulfide inclusion (70 μm across) in zircon Zr-23. Note expansion cracks filled with a sulfide film.

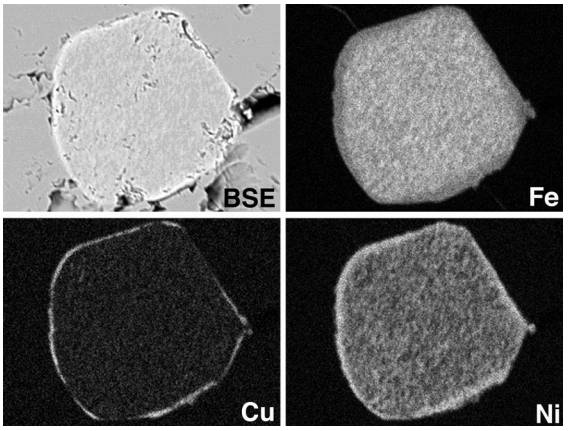

Fig. 3. Backscattered electron (BSE) image and X-ray distribution maps of sulfide inclusion shown in Fig. 1b. Note thin concentric rims of chalcopyrite and pentlandite, surrounding a core of finely intergrown Ni-rich and Ni-poor Mss.

forms (Fig. 2). The sulfide inclusion in sample #4 is an Fe–Ni monosulfide solution (Mss) and that in sample #23 consists of Fe–Ni Mss with pentlandite and chalcopyrite rims (Fig. 3). Microprobe analyses (Table 6) show that the sulfide inclusions are enriched in Ni and hence probably belong to the ultramafic paragenesis [24]. Ponomarenko [2] described a sulfide inclusion consisting of separate blocks of pyrrothite and pentlandite in a Mir zircon; its composition (Table 2) is high in iron compared to those analyzed here.

4.3. U–Pb age data

U–Pb dating of the zircons revealed a narrow spread in age. Twenty-six analyses of 23 grains yielded $^{206}Pb/^{238}U$ ages ranging from 346 to 395 Ma (Table 7). The distribution of points on the reverse concordia ('Tera-Wasserburg') plot (Fig. 4a) suggests that several grains contain common Pb (i.e. lie well above concordia) and two of these also may have experienced minor recent Pb loss. Those grains have been rejected for further age calculation (Fig. 4b, Table 7). The remaining 20 analyses fall within error of the mean, and give a weighted mean $^{206}Pb/^{238}U$ age of 353.6 ± 2.5 Ma (MSWD = 0.53). If all analyses but Mir-6 are included, the weighted mean $^{206}Pb/^{238}U$ age is 355.3 ± 2.3 Ma (MSWD = 0.94). Either age is in reasonable agreement with conventional U–Pb dating of a Mir zircon, which gave a $^{206}Pb/^{238}U$ age of 361.5 Ma [4].

4.4. Hf isotope data

The zircons from Mir show a narrow range in

Table 5
Analyses of silicate and oxide inclusions in zircons from Mir kimberlites

Mineral	Chromite									Cr-Diopside		Olivine
Sample	Zr1			Zr3		Zr21				Zr10		Mz-13
Analysis	core 1	rim 2	small 4	core 5	rim 6	core 7	rim 8	core 9	rim 10	core 11	rim 13	14
SiO_2	0.03	0.03	0.03	0.05	0.02	0.04	0.04	0.00	0.02	54.94	54.79	38.78
TiO_2	3.26	3.05	3.06	3.03	2.87	3.30	2.81	3.30	3.29	0.16	0.12	0.05
Al_2O_3	3.44	3.44	3.40	3.66	3.69	3.23	2.72	3.19	3.15	2.24	2.23	0.36
Cr_2O_3	50.08	48.67	48.17	45.67	45.33	47.05	46.74	46.75	46.78	1.89	1.78	0.06
Fe_2O_3	13.08	13.42	13.31	14.68	14.63	14.00	14.54	14.41	14.73	n.a.	n.a.	n.a.
FeO	21.56	20.35	20.67	20.62	20.58	21.73	20.96	21.64	21.40	n.a.	n.a.	8.17
MnO	0.49	0.48	0.50	0.52	0.48	0.51	0.50	0.44	0.47	0.04	0.01	n.a.
MgO	9.06	9.16	8.73	8.68	8.43	8.23	8.04	8.30	8.47	14.62	14.89	54.14
CaO	0.00	0.00	0.00	0.00	0.00	0.01	0.00	0.00	0.00	20.79	20.44	0.00
Na_2O	0.08	0.04	0.00	0.08	0.08	0.00	0.03	0.03	0.02	2.83	3.13	n.a.
K_2O	0.01	0.00	0.01	0.00	0.00	0.03	0.00	0.00	0.00	0.01	0.00	n.a.
Total	101.09	98.64	97.87	96.99	96.09	98.11	96.39	98.06	98.33	99.63	99.50	101.58

Data for olivine (Mz-13) from Ponomarenko [2].

Table 6
Analyses of sulfide inclusions in zircons from Mir kimberlites

Sample:	Zr-4		Zr-23				Mz-13
Analysis No:	1	2	3	4	5	6	7
Fe	39.69	39.94	40.97	49.30	40.65	28.29	54.04
Co	0.46	0.52	0.60	0.20	0.36	0.41	0.11
Ni	19.82	19.19	19.06	11.03	21.28	34.66	4.03
Cu	1.81	2.40	0.62	0.38	2.87	1.23	0.01
Zn	0.00	0.05	0.00	0.02	0.06	0.00	n.a.
K	0.00	0.01	0.02	0.01	0.02	0.01	n.a.
S	37.48	37.25	37.17	38.57	36.68	31.59	40.43
O	0.38	0.40	0.45	0.12	0.38	0.47	n.a.
Total	99.64	99.78	98.89	99.63	102.31	96.66	98.62

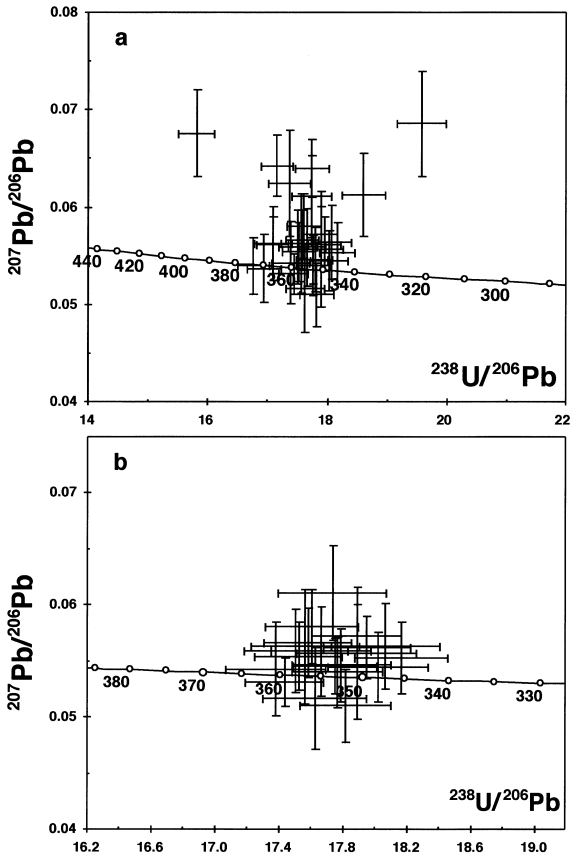

Fig. 4. U–Pb data on Mir zircon megacrysts. (a) Tera-Wasserburg (or 'inverse concordia'; error crosses are 1σ) plot of the zircon population from the Mir kimberlites. (b) Data accepted for age calculation.

Hf isotope composition. $^{176}Hf/^{177}Hf$ varies from 0.28263 to 0.28279, corresponding to a range of ε_{Hf} from +3.0 to +9.2 (Table 8). The ε_{Hf} of zircons from other Siberian kimberlites ranges from +4.4 to +8.6 (except for the Vostok kimberlite, where the zircons have ε_{Hf} from −4.7 to −6.0 [14]). The model ages (T_{DM}) of the Mir zircons range from 600 to 800 Ma, and represent maximum probable ages for the crystallization of the zircons.

4.5. Re–Os data

We have analyzed the three largest sulfide inclusions in the zircons (Table 9). They show a limited range in Os and Pt contents, and low Re/Os ratios (Table 9). T_{RD} model ages (which assume that any Re present represents a late addition) range from 2.37 ± 0.12 to 2.92 ± 0.15 Ga. Because Re/Os ratios are low, the T_{MA} model ages, which accept the measured Re/Os ratios as primary, range from 2.39 ± 0.12 to 3.19 ± 0.15 Ga (mean 2.8 Ga). These values are similar to those determined by Pearson et al. [25] on sulfide inclusions in diamonds from the Udachnaya pipe, and to those determined for 52 low-Re/Os sulfide inclusions in olivine macrocrysts from the Udachnaya pipe [17,26], most of which range from 2.5 to 3.5 Ga. The T_{RD} model ages represent minimum estimates for the time that these sulfides have been isolated from the depleted mantle.

Table 7
LAM-ICPMS U–Pb data for Mir zircons

	U–Th–Pb ratios								Ages (Ma)							
Analysis	207/206	R.S.D.	206/238	R.S.D.	207/235	R.S.D.	208/232	R.S.D.	207/206	±2 S.D.	206/238	±2 S.D.	207/235	±2 S.D.	208/232	±2 S.D.
Mir-1	0.0562	5.0	0.0557	1.51	0.4318	4.9	0.0230	5.0	460	215	350	10	364	30	460	45
Mir-2	0.0546	4.6	0.0563	1.47	0.4238	4.5	0.0209	6.0	394	198	353	10	359	27	417	50
Mir-3	0.0553	5.8	0.0551	1.62	0.4194	5.7	0.0210	6.2	422	248	346	11	356	34	421	52
Mir-4	0.0559	7.1	0.0566	1.77	0.4361	7.0	0.0231	9.0	447	301	355	12	368	43	463	82
Mir-5	0.0581	5.7	0.0568	1.64	0.4550	5.6	0.0262	6.3	533	242	356	11	381	36	522	65
Mir-6	0.0676	6.6	0.0632	1.91	0.5893	6.5	0.0326	10.3	*856*	264	395	15	470	49	649	131
Mir-7	0.0545	5.6	0.0555	1.73	0.4166	5.5	0.0197	6.7	390	242	348	12	354	33	395	52
Mir-8	0.0546	6.0	0.0562	1.73	0.4233	5.9	0.0212	8.6	396	260	353	12	358	36	424	72
Mir-9	0.0554	5.5	0.0571	1.56	0.4359	5.4	0.0194	8.2	428	236	358	11	367	33	389	63
Mir-10	0.0531	4.0	0.0574	1.39	0.4200	3.9	0.0184	4.8	334	177	360	10	356	24	369	35
Mir-11	0.0566	5.5	0.0569	1.56	0.4441	5.4	0.0199	8.8	476	235	357	11	373	34	399	70
Mir-12	0.0643	4.9	0.0583	1.56	0.5163	4.8	0.0262	7.0	*750*	202	365	11	423	33	523	72
Mir-13	0.0561	5.2	0.0585	1.59	0.4528	5.1	0.0231	7.5	*456*	222	367	11	379	32	462	69
Mir-15	0.0557	10.6	0.0559	2.09	0.4291	10.4	0.0336	11.3	439	439	351	14	363	64	668	149
Mir-16	0.0564	6.8	0.0554	1.86	0.4301	6.6	0.0191	10.4	465	288	347	13	363	40	382	79
Mir-17	0.0562	6.8	0.0585	1.81	0.4534	6.6	*0.0205*	9.7	*460*	288	367	13	380	42	410	79
Mir-18A	0.0510	6.4	0.0561	1.59	0.3946	6.3	0.0209	6.9	241	280	352	11	338	36	417	57
Mir-18B	0.0540	5.8	0.0563	1.60	0.4191	5.7	0.0175	6.8	371	249	353	11	355	34	351	48
Mir-18C	0.0625	8.7	0.0576	2.01	0.4960	8.6	0.0259	12.9	*690*	351	361	14	409	58	517	132
Mir-18D	0.0563	9.2	0.0569	1.93	0.4417	9.0	0.0329	10.0	462	384	357	13	371	56	655	128
Mir-19	0.0559	6.7	0.0571	1.86	0.4403	6.6	0.0189	8.1	448	286	358	13	371	41	378	60
Mir-20	0.0572	4.9	0.0559	1.56	0.4413	4.8	0.0222	7.4	500	210	351	11	371	30	443	64
Mir-21	0.0543	7.7	0.0575	1.79	0.4307	7.6	0.0231	10.4	383	328	361	13	364	46	461	95
Mir-22	0.0640	4.7	0.0564	1.58	0.4972	4.6	0.0206	7.8	741	193	354	11	410	31	412	63
Mir-23	0.0611	6.9	0.0564	1.92	0.4748	6.7	0.0227	11.6	*642*	282	354	13	395	44	453	104
Mir-24	0.0516	8.8	0.0567	1.83	0.4039	8.7	0.0264	11.7	269	379	356	13	345	51	526	122

Rejected data in italics.

Table 8
Hf isotope data for Mir zircons

Analysis	$^{176}Hf/^{177}Hf$	2 S.E.M.	$^{176}Lu/^{177}Hf$	$^{176}Yb/^{177}Hf$	T_{DM} (Ga)	ε_{Hf}
Mir-1	0.282794	0.000014	2.2059E-05	7.2790E-04	0.61	8.7
Mir-2	0.282629	0.000017	3.1318E-05	8.5269E-04	0.83	3.0
Mir-3	0.282674	0.000015	1.8317E-05	5.6739E-04	0.77	4.4
Mir-4	0.282744	0.000014	1.2974E-05	3.6487E-04	0.68	7.1
Mir-5	0.282751	0.000015	2.1903E-05	6.5378E-04	0.67	7.4
Mir-6	0.282779	0.000014	3.6735E-06	1.0284E-04	0.63	9.2
Mir-7	0.282734	0.000010	9.4199E-06	2.8371E-04	0.69	6.6
Mir-8	0.282793	0.000010	1.9425E-05	5.8424E-04	0.61	8.8
Mir-9	0.282760	0.000009	1.9510E-05	5.7164E-04	0.66	7.7
Mir-10	0.282751	0.000015	2.6895E-05	8.1523E-04	0.67	7.4
Mir-11	0.282792	0.000014	1.7067E-05	4.9991E-04	0.61	8.8
Mir-12	0.282764	0.000015	1.9472E-05	5.4884E-04	0.65	8.0
Mir-13	0.282755	0.000007	2.5738E-05	8.4142E-04	0.66	7.7
Mir-15	0.282644	0.000010	2.3056E-06	7.5565E-05	0.81	3.4
Mir-16	0.282756	0.000013	1.3472E-05	3.9892E-04	0.66	7.3
Mir-17	0.282791	0.000015	1.5778E-05	5.1708E-04	0.62	9.0
Mir-18	0.282682	0.000011	1.8491E-05	5.5239E-04	0.76	4.8
Mir-19	0.282688	0.000013	1.3587E-05	4.5332E-04	0.75	5.2
Mir-20	0.282728	0.000012	1.2108E-05	3.8239E-04	0.70	6.4
Mir-21	0.282739	0.000014	1.7640E-05	5.5050E-04	0.69	7.0
Mir-23	0.282693	0.000013	1.1121E-05	3.1117E-04	0.75	5.2
Mir-24	0.282725	0.000014	4.5687E-06	1.4460E-04	0.70	6.4
Mir-25	0.282727	0.000011	4.1695E-06	1.3731E-04	0.70	6.5

5. Discussion

The data presented above raise two major questions: (1) when and where were the zircon megacrysts formed, and (2) what is the significance of the difference between the Phanerozoic U–Pb and Hf model ages of the zircon and the Archean Re–Os model ages of the included sulfides?

5.1. Paragenetic association of zircon megacrysts

It is generally accepted that zircon macrocrysts in southern African kimberlites are part of the low-Cr suite of megacrysts (Fe-rich Ol+Opx+Cpx+Gnt ± Ilm ± Phl ± Zir) found in many kimberlites worldwide [7]. This distinctive suite of Cr-poor, Fe-rich megacrysts has been interpreted as crystallized from a highly evolved liquid that may or may not be related to the parental magma of the kimberlite [7,27]. The mantle origin of such zircon megacrysts is apparent from their morphology, their unusual trace element composition, and the composition of the included or intergrown phases, but the origin of the megacryst-forming magmas is still not resolved.

CL images show that the zircon megacrysts are mostly homogeneous single crystals. These crystals commonly have broken surfaces, show plastic deformation and usually are strongly corroded and resorbed. These observations, and particularly the plastic deformation, suggest that the zircons were enclosed in solid rock before they were entrained in the kimberlites.

Unlike the southern African kimberlite zircons, the zircon megacrysts in the Mir pipe have not been found intergrown with other megacryst phases such as ilmenite and Fe-rich olivine. Instead, the predominant inclusions are Ti-rich chromites, and chrome diopside and Ni-rich sulfides also are present. Magnesian olivine ([2], Table 5) and rare phlogopite [28] also have been described as inclusions in Mir zircons. These data suggest that the zircon megacryst population in the Mir pipe was formed in a peridotitic (lher-

zolitic) environment, in contrast to the zircon megacrysts from Monastery or other kimberlite pipes of South Africa. The presence of large (and apparently abundant) zircon in a peridotitic matrix is anomalous, and suggests to us that it is the result of reaction between metasomatic fluids (or melts) and a peridotitic wall rock. This model would be consistent with the presence of phlogopite and the high Ti content of the chromite inclusions, as noted above. It is significant that chromites, chrome diopsides and sulfides similar in composition to those enclosed in Mir zircons also have been found as inclusions in diamonds from this pipe [24,29].

It is difficult to determine the exact *P-T* conditions for the zircon crystallization. The narrow range in composition of the chrome diopside inclusions in the zircon megacrysts, with Ca/(Ca+Mg) = 0.47–0.49, gives a temperature of about 950°C [28]. The large grain size and homogeneity of the zircons suggest they formed under stable conditions.

5.2. Zircon ages and Re–Os ages of sulfide inclusions

Precise emplacement ages of individual diatremes are needed to unravel the extended geochemical and tectonic history of many kimberlite provinces. More than two decades ago Davis et al. [30] established the usefulness of zircon in defining the eruptive ages of southern African kimberlites. The first conventional dating of many kimberlite pipes on the Siberian platform, including the Mir kimberlite pipe, was done four years later [4]. Conventional U–Pb dating of a zircon from the Mir kimberlite [4] gave an age of 361 ± 2 Ma, within the spread of individual ages obtained in this study (346–395 Ma); the results presented here give a weighted mean $^{206}Pb/^{238}U$ age of 353.6 ± 2.5 Ma.

U–Pb ages of mantle-derived zircons have been interpreted as representing the timing of kimberlite emplacement, based on the assumption that the U–Pb system is continuously reset under upper mantle conditions prior to transport to the surface [4]. However, U–Pb ion probe (SHRIMP) results for some mantle zircons demonstrate that old pre-eruption ages can be preserved in some cases [31,32]. Belousova et al. [11] used LAM-ICPMS dating to demonstrate the preservation of Proterozoic U–Pb ages in one population of mantle-derived zircons from the Jurassic Timber Creek kimberlite in Australia. These authors suggested that kimberlitic zircons are likely to retain old U–Pb ages at mantle temperatures, because of their low U and Th contents, which limit the degree of radiation damage to the lattice, and hence the rate of Pb diffusion.

In the present case, the Hf isotope data place further constraints on the interpretation of the age of zircon crystallization. Because of its high Hf contents and low Lu/Hf ratios, zircon essentially retains the initial $^{176}Hf/^{177}Hf$ of the medium from which it grew, and is resistant to recrystallization. The T_{DM} model ages represent the maximum time at which the host magma of the zircons could have separated from a depleted mantle source, and hence a maximum age of zircon crystallization. Griffin et al. [14] suggested that the Hf isotope composition of kimberlitic zircons reflects mixing between the Hf in their parental melts or fluids, derived from a depleted mantle source, and ancient unradiogenic Hf in the peridotitic wall rocks. Any contamination of the host magma with older lithospheric Hf thus would raise the apparent T_{DM} of the zircon [14]. The model presented here provides a mechanism for achieving

Table 9
Re–Os data for sulfide inclusions in Mir zircons

Sample	$^{187}Os/^{188}Os$	±2 S.E.M.	$^{187}Re/^{188}Os$	±2 S.E.M.	Os (ppm)	Pt (ppm)	T_{RD} (Ga)	T_{MA} (Ga)	±2 S.D.
Zr-M4	0.10798	0.00026	0.00856	0.00003	103	7	2.78	2.84	0.04
Zr-M6	0.11082	0.00086	0.00393	0.00013	259	10	2.37	2.39	0.12
Zr-M23	0.10698	0.00094	0.03527	0.00046	54	3	2.92	3.19	0.15

that mixing as zircon grew within the peridotite; much of the Zr and Hf would be supplied by the metasomatic source, because of the low Zr and Hf content of the peridotite. In this metasomatic model, the Hf isotope composition of the zircon probably is much closer to that of the metasomatic medium than to that of the peridotitic wall rock. In this situation, the lowest model ages are likely to be closest to the crystallization age of the zircon.

We interpret the U–Pb age of the Mir zircons as reflecting the time of their crystallization, and consider this event to have occurred shortly before the eruption of the Mir kimberlite. Alternative interpretations are: (1) the zircons are older, but lost lead continuously up to the time they were 'quenched' by kimberlite eruption, and (2) the zircons are older, but their U–Pb systems were reset by a thermal event correpsonding to the kimberlite eruption. However, regardless of arguments about the rates and causes of Pb loss in mantle zircon, the Hf isotope data constrain the zircon crystallization to $\leq$600–800 Ma.

The Re–Os model ages on the sulfide inclusions are also model dependent, but for the low $^{187}Os/^{188}$ Os and Re/Os ratios reported here, there is little leeway in the calculation of alternative model ages. Sulfide phases are the major residence of Os in mantle peridotites, and Os is a strongly compatible element in the sulfides [34]; the Re–Os systematics of the sulfide phases therefore are difficult to reset. However, an existing sulfide might be modified via metasomatic fluids that carry Re and/or Os; for example, Pearson et al. [17] showed that fluids carrying Re and highly radiogenic Os had affected sulfides in Massif Central peridotite xenoliths. Similarly, a detailed in situ study of sulfide inclusions in olivine macrocrysts (disaggregated peridotites) from the Udachnnaya kimberlite [26] showed that any later metasomatic disturbance of an old sulfide grain is most likely to add more radiogenic Os, with or without Re, and thus to decrease model ages. This process may be reflected in the spread of model ages from the sulfides in the Mir zircons; the slightly younger age and higher Os content of sulfide M6 might represent the addition of radiogenic Os. We therefore interpret these model ages as minimum estimates of the original crystallization age of the sulfides.

If the constraints provided by the U–Pb and Hf data are correct, there is only one reasonable explanation for the much older Re–Os model ages of the sulfide inclusions: the capturing of residual sulfide phases in the host peridotite by the growing zircon crystals. This model implies that the Os isotope composition of the sulfide phases was not seriously altered by interaction with the metasomatic fluids. This is reasonable, because the sulfides have very high Os concentrations, whereas the Os content of most fluids and melts is likely to be low [33], especially if these fluids do not contain a sulfide component [34]. Navon et al. [35] and Schrauder et al. [36] have analyzed fluids trapped in diamonds, and shown that these have very low S contents.

5.3. Implications for the Re–Os dating of diamonds

These results are relevant to the problem of the ages of diamonds. The development of microchemical methods has allowed the determination of highly precise Re–Os model ages on single sulfide inclusions in diamonds [17,25]. Similar results have been obtained by the in situ methods described here [17]. These model ages have been widely interpreted as the age of diamond formation [25,37,38].

However, the ancient Re–Os ages of their sulfide inclusions clearly do not date the formation of the zircon megacrysts studied here. Instead, these data indicate that Phanerozoic metasomatism did not substantially reset the Os isotope composition of peridotitic sulfides, which were enclosed in the metasomatic zircon. A similar phenomenon was observed by Carlson and Bell [39], who reported an Archean Re–Os model age for sulfide inclusions in a kimberlitic clinopyroxene megacryst, believed on other grounds to be Mesozoic in age; in this case Re had been added to the sulfide near the time of kimberlite eruption.

From these observations there follows a direct implication for the dating of diamonds: like the zircons, diamond may simply have overgrown peridotitic (or eclogite) phases, without necessarily modifying their chemical or isotopic composi-

tion. Similarly, diamonds that grew much later, through metasomatic processes, could have captured and inherited old sulfides which date back to the time of peridotite or eclogite formation in the mantle. A similar inference has been drawn on theoretical grounds by Navon [40], who suggested that most model ages (including the Os, Nd and Pb isotopic systems) on diamond inclusion phases reflect heterogeneity in mantle rocks rather than the age of diamond formation.

One common argument for the syngenetic nature of mineral inclusions, including sulfide inclusions, in diamonds is the negative-crystal form of the inclusions. However, non-syngenetic inclusions such as the Mir sulfides also can display well-defined negative-crystal forms (Fig. 2). Sulfides are the most common inclusion phase in diamonds worldwide; this observation and the occurrence of multiple sulfide inclusions in single diamonds have been used to argue that sulfides catalyze the precipitation of diamonds [24,37]. However, in a study of 70 sulfide-bearing olivine macrocrysts (0.5–5 mm) from the Udachnnaya kimberlite, Griffin et al. [26] reported nine grains that contained two sulfide inclusions, and five that contained three to six individual inclusions. Within some of these olivine grains the sulfides showed a wide range of Re–Os model ages, suggesting repeated introduction of sulfide, and recrystallization of the olivine. These observations show that ancient sulfides may occur locally in high concentrations in depleted mantle peridotites, and their occurrence in diamonds is not necessarily evidence of a genetic relationship. The data reported here provide additional support to arguments for the relatively late metasomatic formation of diamond in mantle rocks [41,42].

The range of ages reported for diamond inclusion phases therefore may reflect either multistage growth of diamond in the mantle, or the late growth of diamond in mantle rocks with a long and complex history, or both. Young model ages or isochron ages on diamond inclusions require that some diamonds must be relatively young, whereas the presence of diamonds in ancient sediments leaves little doubt that at least some diamonds are very old. However, the results reported here suggest that Re–Os model ages or isochron ages on sulfide inclusions in diamonds do not obviously date the formation of the diamond itself, and that these ages do not provide precise information on the timing of diamond growth events. In the absence of strong evidence that sulfide inclusions in diamonds are syngenetic, the possibility must be considered that the sulfides formed in mantle rocks and were later captured by diamonds growing in the mantle environment.

6. Conclusions

The zircon megacryst suite from the Mir kimberlite contains an inclusion assemblage distinct from that of southern African kimberlite zircon populations; this assemblage indicates that the zircons crystallized in a metasomatized ultramafic environment. U–Pb and Hf isotope data show the Mir zircon population probably crystallized at 353.6 ± 2.5 Ma (pooled $^{206}Pb/^{238}U$ age) and is unlikely to be older than 600 Ma (minimum Hf isotope model age). However, these zircons contain sulfide inclusions with Re–Os model ages of 2.4–3.2 Ga. This discordance in ages suggests that the zircons, growing metasomatically in a peridotite wall rock, inherited sulfides residual from an ancient depletion event, and that the metasomatic activity did not substantially reset the Os isotope compositions of the sulfides. A corollary of these results is that Re–Os isotopic data from sulfide inclusions in diamonds must be interpreted with caution, as they may not represent the age of the diamonds.

Acknowledgements

We thank Ashwini Sharma for her assistance with LAM-ICPMS analyses, and Natasha Merkulova and Tom Bradley for help in preparing zircon mounts. We are grateful to Alexander Ivanov of ALROSA Co. Ltd. for assistance with the electron microprobe analyses. Ray Burgess, Rick Carlson and Bruce Patterson contributed thoughtful reviews that helped to improve the manuscript. This work was funded by a Macquarie University Research grant and the ARC GEM-

OC Key Centre. This is contribution No. 268 from the ARC National Key Centre for the Geochemical Evolution and Metallogeny of Continents (www.es.mq.edu.au/GEMOC/).*[BW]*

References

[1] A.P. Bobrievich, M.N. Bondarenko, M.A. Gnevushev, A.M. Krasov, G.I. Smirnov, R.K. Yurkevich, The diamond deposits of Yakutia, Gosgeoltekhizdat, Moscow, 1959, 527 pp. (in Russian).

[2] A.I. Ponomarenko, Inclusions of silicates, oxides and sulfides in zircon from kimberlites of pipe 'Mir' (Yakutia), Dokl. Akad. Nauk. SSSR 249 (1978) 1442–1446.

[3] A.I. Botkunov, V.K. Garanin, G.P. Kudriavtseva, M.S. Perminova, Mineral inclusions in zircon from kimberlite pipe 'Mir', Dokl. Akad. Nauk. SSSR 251 (1980) 1233–1236 (in Russian).

[4] G.L. Davis, N.V. Sobolev, A.D. Kharkiv, New data on the age of Yakutian kimberlites obtained by the uranium-lead method on zircons, Dokl. Akad. Nauk. SSSR 254 (1980) 175–180 (in Russian).

[5] T.K. Whitelock, The Monastery mine kimberlite pipe, in: P.H. Nixon (Ed.), Lesotho Kimberlites, Lesotho National Development Corporation, Maseru, 1973, pp. 214–218.

[6] P. Kresten, P. Fels, G. Berggren, Kimberlite zircons – a possible aid in prospecting for kimberlites, Mineral. Depos. (Berlin) 10 (1975) 47–56.

[7] R.O. Moore, W.L. Griffin, J.J. Gurney, C.G. Ryan, D.R. Cousens, S.H. Sie, G.F. Suter, Trace element geochemistry of ilmenite megacrysts from the Monastery kimberlite, South Africa, Lithos 29 (1992) 1–18.

[8] M.D. Norman, N.J. Pearson, A. Sharma, W.L. Griffin, Quantitative analysis of trace elements in geological materials by laser ablation ICPMS: Instrumental operating conditions and calibration values of NIST glasses, Geostand. Newsl. 20 (1996) 247–261.

[9] E.A. Belousova, Trace Elements in Apatite and Zircon: Applications to Petrogenesis and Mineral Exploration, PhD Thesis, Macquarie University, Sydney, 2000, 279 pp.

[10] M.D. Norman, W.L. Griffin, N.J. Pearson, M.O. Garcia, S.Y. O'Reilly, Quantitative analysis of trace element abundances in glasses and minerals: a comparison of laser ablation ICPMS, solution ICPMS, proton microprobe, and electron microprobe data, J. Anal. At. Spectrom. 13 (1998) 477–482.

[11] E.A. Belousova, W.L. Griffin, S.R. Shee, S.E. Jackson, S.Y. O'Reilly, Two age populations of zircons from the Timber Creek kimberlites, Northern territory, Australia as determined by laser-ablation ICPMS analysis, Aust. J. Earth Sci. 48 (2001) 757–766.

[12] T. Hirata, R.W. Nesbitt, U–Pb isotope geochronology of zircon: Evaluation of the laser probe-inductively coupled plasma-mass spectrometry technique, Geochim. Cosmochim. Acta 59 (1995) 2491–2500.

[13] K.R. Ludwig, Isoplot – a geochronological toolkit for Microsoft Excel, Berkeley Geochronology Center, Spec. Publ. No. 1a, 2000, 53 pp.

[14] W.L. Griffin, N.J. Pearson, E.A. Belousova, S.R. Jackson, E. VanAchterbergh, S.Y. O'Reilly, S.R. Shee, The Hf isotope composition of cratonic mantle: LAM-MC-ICPMS analysis of zircon megacrysts in kimberlites, Geochim. Cosmochim. Acta 64 (2000) 133–147.

[15] P. DeBievre, P.D.P. Taylor, Table of the isotopic composition of the elements, Int. J. Mass Spectrom. Ion Process. 123 (1993) 149.

[16] J. Blichert-Toft, F. Albarede, The Lu–Hf geochemistry of chondrites and the evolution of the mantle-crust system, Earth Planet. Sci. Lett. 148 (1997) 243–258; Erratum, Earth Planet. Sci. Lett. 154 (1998) 349.

[17] N.J. Pearson, O. Alard, W.L. Griffin, S.E. Jackson, S.Y. O'Reilly, In situ measurement of Re–Os isotopes in mantle sulfides by laser ablation multi-collector inductively-coupled mass spectrometry: analytical methods and preliminary results, Geochim. Cosmochim. Acta 66 (2002) 1037–1050.

[18] E.A. Belousova, W.L. Griffin, N.J. Pearson, Trace element composition and cathodoluminescence properties of southern African kimberlitic zircons, Mineral. Mag. 62 (1998) 355–366.

[19] E.A. Belousova, W.L. Griffin, S.Y. O'Reilly, Cathodoluminescence and geochemical properties of kimberlitic and lamproitic zircons, 7th Int. Kimberlite Conf. Proc., Cape Town, 1999, pp. 23–29.

[20] W.L. Griffin, C.G. Ryan, J.J. Gurney, N.V. Sobolev, Chromite macrocrysts in kimberlites and lamproites: geochemistry and origin, in: H.O.A. Meyer, O.H. Leonardos (Eds.), Kimberlites, Related Rocks and Mantle Xenoliths, CPRM Spec. Publ. 1A/93, 1994, pp. 366–377.

[21] D.J. Schulze, Chromite macrocrysts from southern African kimberlites: mantle xenolith sources and post-diamond re-equilibration, Africa, Geosci. Rev. 3 (1996) 203–216.

[22] W.L. Griffin, C.G. Ryan, Trace elements in indicator minerals: Area selection and target evaluation in diamond exploration, J. Geochem. Explor. 53 (1995) 311–337.

[23] Z.V. Spetsius, V.P. Serenko, Composition of Continental Upper Mantle and Lower Crust Beneath the Siberian Platform, Nauka, Moscow, 1990, 272 pp. (in Russian).

[24] G. Bulanova, W.L. Griffin, C.G. Ryan, Trace elements in sulfide inclusions from Yakutian diamonds, Contrib. Mineral. Petrol. 124 (1996) 111–125.

[25] D.G. Pearson, S.B. Shirey, J.W. Harris, R.W. Carlson, Sulphide inclusions in diamonds from the Koffiefontein kimberlite, S. Africa: constraints on diamond ages and mantle Re–Os systematics, Earth Planet. Sci. Lett. 160 (1998) 311–326.

[26] W.L Griffin, Z.V. Spetsius, N.J. Pearson, S.Y. O'Reilly, In-situ Re–Os analysis of sulfide inclusions in kimberlitic olivine: new constraints on depletion events in the Siberian lithospheric mantle, Geochem. Geophys. Geosyst. (2001), submitted.

[27] J.J. Gurney, W.R.O. Jakob, J.B. Dawson, Megacrysts from the Monastery kimberlite pipe, South Africa, in: F.R. Boyd, H.O.A. Meyer (Eds.), The Mantle Sample: Inclusions in Kimberlites and Other Volcanics, AGU, Washington, DC, 1979, pp. 227–243.

[28] V.K. Garanin, F.I. Kasimova, F.P. Melnikov, The temperature formation of zircon and its paragenic associations from Mir kimberlite pipe, Izv. VUZOV, Geol. Explor. 1 (1993) 67–70 (in Russian).

[29] N.V Sobolev, Deep-seated Inclusions in Kimberlites and the Problem of the Composition of the Upper Mantle, Nauka, Novosibirsk, 1974, 263 pp. (in Russian), English Translation by D.A. Brown, F.R. Boyd (Eds.), AGU, Washington, DC, 1977, 279 pp.

[30] G.L. Davis, T.E. Krogh, A.J. Erlank, The age of zircons from kimberlites from South Africa, Carnegie Inst. Year Bk. 75 (1976) 821–824.

[31] P.D. Kinny, W. Compston, J.W. Bristow, I.S. Williams, Archean mantle xenocrysts in a Permian kimberlite: Two generations of kimberlitic zircon in Jwaneng DK2, southern Botswana, Geol. Soc. Aust. Spec. Publ. 14 (1989) 833–842.

[32] P.D. Kinny, H.O.A. Meyer, Zircons from the mantle: a new way to date old diamonds, J. Geol. 102 (1994) 475–481.

[33] S.B. Shirey, R.J. Walker, The Re–Os isotope system in cosmochemistry and high-temperature geochemistry, Annu. Rev. Earth Planet. Sci. 26 (1998) 423–500.

[34] O. Alard, W.L. Griffin, J.P. Lorand, S.E. Jackson, S.Y. O'Reilly, Non-chondritic distribution of the highly siderophile elements in mantle sulfides, Nature 407 (2000) 891–894.

[35] O. Navon, I.D. Hutcheon, G.R. Rossman, G.J. Wasserburg, Mantle-derived fluids in diamond micro-inclusions, Nature 335 (1989) 784–789.

[36] M. Schrauder, C. Koeberl, O. Navon, Trace element analysis of fluid-bearing diamonds from Jwaneng (Botswana), Geochim. Cosmochim. Acta 60 (1996) 4711–4724.

[37] D.G. Pearson, S.B. Shirey, G.P. Bulanova, R.W. Carlson, H.J. Milledge, Re–Os isotopic measurements of single sulfide inclusions in a Siberian diamond and its nitrogen aggregation systematics, Geochim. Cosmochim. Acta 63 (1999) 703–711.

[38] S.B. Shirey, R.W. Carlson, S.H. Richardson, A. Menzies, J. Gurney, D.G. Pearson, J.W. Harris, U. Wiechert, Archean emplacement of eclogitic components into the lithospheric mantle during formation of the Kaapvaal Craton, Geophys. Res. Lett. 28 (2001) 2509–2512.

[39] R.W. Carlson, D.R. Bell, Rhenium–osmium systematics of kimberlite megacryst inclusions: implications for the source of kimberlitic magmas, Ext. Abstr., 7th Annu. V.M. Goldschmidt Conference, Tucson, AZ, 1997, pp. 43–44.

[40] O. Navon, Diamond formation in the Earth's mantle, 7th Int. Kimberlite Conf. Proc., Cape Town, 1999, pp. 584–604.

[41] Z.V. Spetsius, Two generation of diamonds in the eclogite xenoliths, Proc. 7th Int. Kimberlite Conf., Cape Town, 1999, pp. 823–828.

[42] L.A. Taylor, G.P. Bulanova, H.J. Milledge, G.A. Snyder, R.A. Keller, Metasomatic eclogitic diamond growth: Evidence from multiple inclusions, Int. Geol. Rev. 40 (1998) 592–604.

[43] N. Machado, G. Gauthier, Determination of 207Pb/206Pb ages on zircon and monazite by laser-ablation ICPMS and application to a study of sedimentary provenance and metamorphism of southeastern Brazil, Geochim. Cosmochim. Acta 60 (1996) 5063–5073.

[44] M. Wiedenbeck, P. Alle, F. Corfu, W.L. Griffin, M. Meier, F. Oberli, A. VonQuart, J.C. Roddick, W. Spiegel, Three natural zircon standards for U–Th–Ph, Lu–Th, trace element and REE analyses, Geostand. Newsl. 19 (1995) 1–23.

[45] L.P. Black, B.L. Gulson, The Age of the Mud Tank carbonatite, Strangways Range, Northern Territory, BMR J. Aust. Geol. Geophys. 3 (1978) 227–232.